

Quasielastic scattering with the Relativistic Green's Function approach

Andrea Meucci and Carlotta Giusti

*Dipartimento di Fisica - Università degli Studi di Pavia
and INFN - Sezione di Pavia, via A. Bassi 6, I-27100 Pavia, Italy*

Abstract. A relativistic model for quasielastic (QE) lepton-nucleus scattering is presented. The effects of final-state interactions (FSI) between the ejected nucleon and the residual nucleus are described in the relativistic Green's function (RGF) model where FSI are consistently described with exclusive scattering using a complex optical potential. The results of the model are compared with experimental results of electron and neutrino scattering.

Keywords: Relativistic models, Electron scattering, Neutrino scattering

PACS: 25.30.Pt; 25.30.Fj; 13.15.+g; 24.10.Jv

FINAL-STATE INTERACTIONS IN LEPTON-NUCLEUS SCATTERING

In the QE region the nuclear response to an electroweak probe is dominated by one-nucleon knockout processes, where the scattering occurs with only one nucleon while the remaining nucleons of the target behave as simple spectators. The reaction can adequately be described in the relativistic impulse approximation (IA) by the sum of incoherent processes involving only one nucleon scattering and the components of the hadron tensor are obtained from the sum, over all the single-particle (s.p.) shell-model states, of the squared absolute value of the transition matrix elements of the single-nucleon current. A reliable description of FSI is an essential ingredient for the comparison with data. The relevance of FSI has been clearly stated for the exclusive $(e, e'p)$ reaction, where the use of complex optical potentials (OP) in the distorted-wave impulse approximation (DWIA) is required [1, 2, 3, 4, 5, 6, 7, 8]. The imaginary part of the OP produces an absorption that reduces the cross section and accounts for the fact that, if other channels are open besides the elastic one, part of the incident flux is lost in the elastically scattered beam and goes to the other (inelastic) channels which are open. In the inclusive scattering only the emitted lepton is detected, the final nuclear state is not determined and all elastic and inelastic channels contribute. This requires a different treatment of FSI where all final-state channels should be retained and the total flux, although redistributed among all possible channels, must be conserved. Different approaches have been used to describe FSI in relativistic calculations for the inclusive QE electron- and neutrino-nucleus scattering. In the relativistic plane-wave impulse approximation (RPWIA), FSI are simply neglected. In another approach, FSI are accounted for in relativistic DWIA (RDWIA) calculations by including only the real part of the relativistic optical potential (rROP).

In the RGF techniques [9, 10, 11, 12, 13, 14, 15, 16, 17, 18, 19], FSI are described in the inclusive scattering by the same complex OP as in the exclusive scattering, but the imaginary part is used in the two cases in a different way and in the inclusive reaction the flux, although is redistributed in all the channels, is conserved. In the RGF model with suitable approximations, which are mainly related to the impulse approximation, the components of the hadron tensor are written in terms of the s.p. optical model Green's function. The explicit calculation of the s.p. Green's function can be avoided by its spectral representation, which is based on a biorthogonal expansion in terms of the eigenfunctions of the non-Hermitian optical potential and of its Hermitian conjugate

$$[\mathcal{E} - T - \mathcal{V}^\dagger(E)] | \chi_{\mathcal{E}}^{(-)}(E) \rangle = 0, \quad [\mathcal{E} - T - \mathcal{V}(E)] | \tilde{\chi}_{\mathcal{E}}^{(-)}(E) \rangle = 0. \quad (1)$$

The expanded form for the s.p. expression of the hadron tensor components is [10, 11]

$$W^{\mu\nu}(q, \omega) = \sum_n \left[\text{Re } T_n^{\mu\nu}(E_f - \varepsilon_n, E_f - \varepsilon_n) - \frac{1}{\pi} \mathcal{P} \int_M^\infty d\mathcal{E} \frac{1}{E_f - \varepsilon_n - \mathcal{E}} \text{Im } T_n^{\mu\nu}(\mathcal{E}, E_f - \varepsilon_n) \right], \quad (2)$$

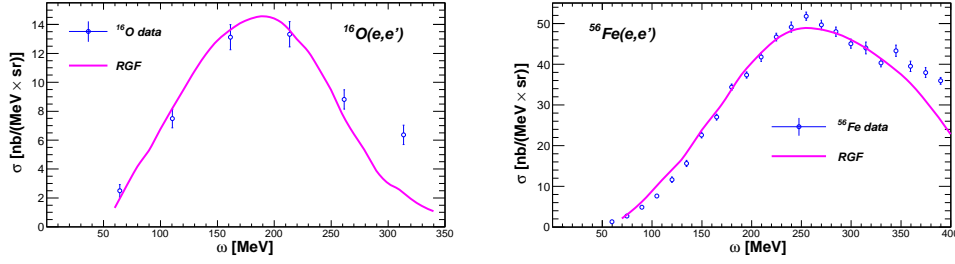


FIGURE 1. Differential cross section of the reactions $^{16}\text{O}(e, e')$ for beam energy $\varepsilon = 1080$ MeV and scattering angle $\vartheta = 32^\circ$ and $^{56}\text{Fe}(e, e')$ for beam energy $\varepsilon = 2020$ MeV and scattering angle $\vartheta = 20^\circ$. Experimental data from [25] (^{16}O) and [26] (^{56}Fe).

where \mathcal{P} denotes the principal value of the integral, n is the eigenstate of the residual nucleus with energy ε_n , and

$$T_n^{\mu\mu}(\mathcal{E}, E) = \lambda_n \langle \varphi_n | j^{\mu\dagger}(\mathbf{q}) \sqrt{1 - \mathcal{V}'(E)} | \tilde{\chi}_{\mathcal{E}}^{(-)}(E) \rangle \langle \chi_{\mathcal{E}}^{(-)}(E) | \sqrt{1 - \mathcal{V}'(E)} j^{\mu}(\mathbf{q}) | \varphi_n \rangle, \quad (3)$$

and similar expressions for the terms with $\mu \neq \nu$. The factor $\sqrt{1 - \mathcal{V}'(E)}$, where $\mathcal{V}'(E)$ is the energy derivative of the optical potential, accounts for interference effects between different channels and allows the replacement of the mean field \mathcal{V} with the phenomenological OP.

Disregarding the square root correction, the second matrix element in Eq. (3) is the transition amplitude for the single-nucleon knockout from a nucleus in the state $|\Psi_0\rangle$ leaving the residual nucleus in the state $|n\rangle$ and it is similar to the usual DWIA expression for the transition amplitude of the exclusive single-nucleon knockout, i.e., the imaginary part of \mathcal{V}^\dagger gives an attenuation of the strength that is inconsistent with the inclusive process, where all the inelastic channels must be considered and the total flux must be conserved. This compensation is performed by the first matrix element in the right hand side of Eq. (3), which involves the eigenfunction $\tilde{\chi}_{\mathcal{E}}^{(-)}(E)$ of the Hermitian conjugate optical potential, where the imaginary part has an opposite sign and has the effect of increasing the strength. Therefore, in the RGF approach the imaginary part of the optical potential redistributes the flux lost in a channel in the other channels, and in the sum over n the total flux is conserved. The RGF model requires the calculations of matrix elements of the same type as in usual RDWIA models, but involves eigenfunctions of both \mathcal{V} and \mathcal{V}^\dagger : FSI are described by the same complex optical potential as in RDWIA thus providing a consistent treatment of FSI in the exclusive and in the inclusive scattering.

RESULTS FOR ELECTRON AND NEUTRINO SCATTERING

The first measurement of the charged-current quasielastic (CCQE) flux-averaged double-differential muon neutrino cross section on ^{12}C in an energy range up to ≈ 3 GeV that have been reported by the MiniBooNE Collaboration [20] have raised extensive discussions. In particular, the experimental cross section is usually underestimated by the relativistic Fermi gas model and by other more sophisticated models based on the IA [21, 22, 23], unless the nucleon axial mass M_A is significantly enlarged with respect to the world average value of $1.03 \text{ GeV}/c^2$. Despite the fact the larger axial mass obtained from the MiniBooNE data on carbon can be interpreted as an effective way to include medium effects which are not taken into account, it is clear that, before drawing conclusions, a precise knowledge of lepton-nucleus cross sections, where uncertainties on nuclear effects are reduced as much as possible, is necessary. Moreover, any reliable calculation for neutrino scattering should first be tested against electron scattering in the same kinematical conditions.

In this section several results obtained with the RGF model for electron and neutrino-nucleus scattering are discussed. Some results of the RGF for inclusive electron and neutrino scattering are presented in [16, 18], where they are compared with the results obtained with the relativistic mean field model [24], which uses the same strong real potential already considered in describing the bound states to evaluate the scattering wave functions.

As an example, in Fig. 1 the RGF results are compared with the experimental (e, e') cross section on ^{16}O and ^{56}Fe . In all the calculations presented here the bound nucleon states are self-consistent Dirac-Hartree solutions derived within a relativistic mean-field approach [27], and in the RGF different parameterizations have been used for the relativistic optical potential: the energy-dependent and A-dependent (where A is the mass number) EDAD1 and the

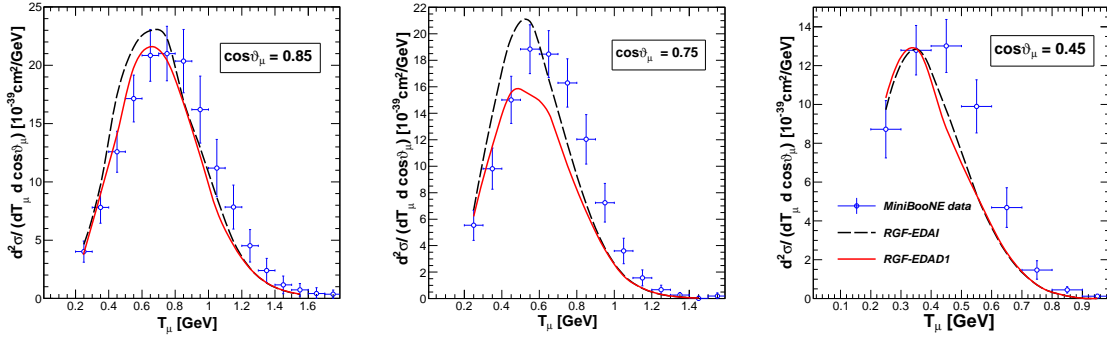


FIGURE 2. Flux-averaged double-differential cross section per target nucleon for the CCQE $^{12}\text{C}(\nu_\mu, \mu^-)$ reaction calculated with the RGF-EDAI (dashed lines) and the RGF-EDAD1 (solid lines) displayed versus T_μ for three bins of $\cos\vartheta_\mu$. The data are from MiniBooNE [20].

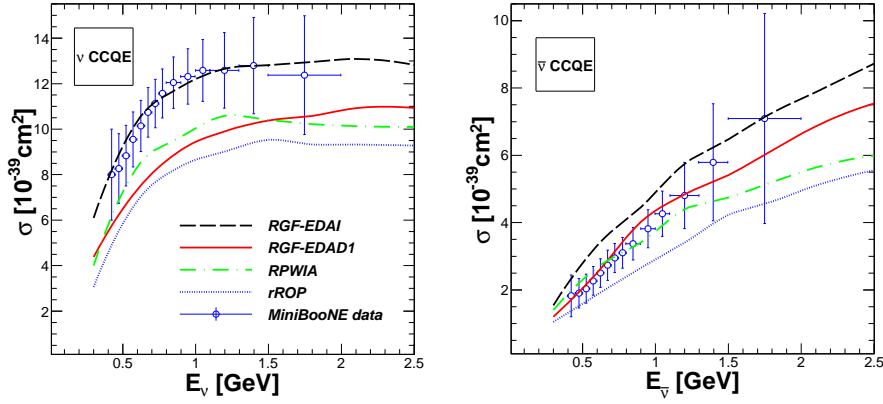


FIGURE 3. Total CCQE cross section per target nucleon as a function of E_ν (left panel) and $E_{\bar{\nu}}$ (right panel) calculated with the RGF-EDAD1 (solid line), the RGF-EDAI (dashed line), the rROP (dotted line), and the RPWIA (dot-dashed line). The data are from MiniBooNE [20, 29].

energy-dependent but A -independent EDAI complex phenomenological potentials of [28]. The shape followed by the RGF cross sections fits well the slope shown by the data, in particular approaching the peak region, where the RGF produces cross sections in reasonable agreement with the data. Although satisfactory on general grounds, the comparison with data in Fig. 1 cannot be conclusive until contributions beyond the QE peak, like meson exchange currents and Δ effects, which may play a significant role in the analysis of data even at the maximum of the QE peak, are carefully evaluated.

In Fig. 2 the CCQE double-differential $^{12}\text{C}(\nu_\mu, \mu^-)$ cross sections averaged over the neutrino flux is displayed as a function of the muon kinetic energy T_μ for three bins of $\cos\vartheta_\mu$, where ϑ_μ is the muon scattering angle. In all the calculations of neutrino-nucleus scattering the standard value of the nucleon axial mass, i.e., $M_A = 1.03 \text{ GeV}/c^2$ has been used. A good agreement with the MiniBooNE data of [20] is generally shown by the RGF cross sections [18]. The differences between the RGF results with the two optical potentials are enhanced in the peak region but they always are of the order of the experimental errors. The EDAD1 and EDAI potentials yield close predictions for the bin $0.4 \leq \cos\vartheta_\mu \leq 0.5$; small differences are seen in the bin $0.8 \leq \cos\vartheta_\mu \leq 0.9$, while larger differences can be found for the bin $0.7 \leq \cos\vartheta_\mu \leq 0.8$. Nevertheless, the RGF-EDAI cross section is always larger than the RGF-EDAD1 one. The differences between the RGF-EDAI and the RGF-EDAD1 results are due to the different imaginary parts.

In Fig. 3 the total CCQE cross sections per target nucleon for neutrino and antineutrino scattering are displayed as functions of the neutrino or antineutrino energies E_ν and $E_{\bar{\nu}}$ and compared with the “unfolded” MiniBooNE data [20, 29]. The RPWIA and rROP results usually underpredict the ν_μ data. Larger cross sections, in particular for larger

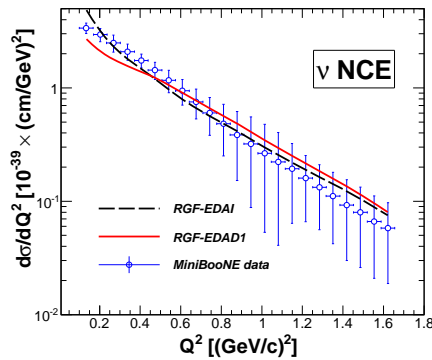


FIGURE 4. NCE flux-averaged cross section per target nucleon as a function of Q^2 calculated with the RGF-EDAD1 (solid line) and the RGF-EDAI (dashed line). The data are from MiniBooNE [30].

values of E_ν , are obtained in the RGF with both optical potentials [18]. The differences between the RGF-EDAI and the RGF-EDAD1 results, being RGF-EDAI in good agreement with the shape and magnitude of the ν_μ data, are due to the different imaginary parts. The enhancement of the RGF cross sections is due to the translation to the inclusive strength of the overall effect of inelastic channels which are not incorporated in other models based on the IA.

The total CCQE cross section for $\bar{\nu}_\mu$ scattering is displayed in the right panel of Fig. 3. Also in this case the RGF results are usually larger than the RPWIA and rROP ones. The differences between the RGF-EDAD1 and RGF-EDAI results are significant but somewhat smaller than for neutrino scattering. A reasonable agreement with the experimental data is obtained, but the RGF-EDAI calculations are larger than the data up to $E_{\bar{\nu}} \approx 1.5$ GeV, while a better agreement is obtained with the RGF-EDAD1 ones. The different behavior of the cross sections for neutrino and antineutrino scattering is related to the relative strength of the vector-axial response, which is constructive in ν scattering and destructive in $\bar{\nu}$ scattering, with respect to the longitudinal and transverse ones [19].

The MiniBooNE Collaboration has reported [30] also a measurement of the flux-averaged differential cross section as a function of the four-momentum transferred squared, $Q^2 = -q^\mu q_\mu$, for neutral-current elastic (NCE) neutrino scattering on CH_2 in a Q^2 range up to ≈ 1.65 $(\text{GeV}/c)^2$. The analysis of ν -nucleus NCE reactions introduces additional complications, as the final neutrino cannot be measured and a final hadron has to be detected: the cross sections are therefore semi-inclusive in the hadronic sector and inclusive in the leptonic one [31, 32, 33]. Different relativistic descriptions of FSI are compared with the NCE MiniBooNE data in [34], while in Fig. 4 we show our RGF results calculated with both EDAI and EDAD1 potentials. Also in this case, the RGF produces large cross sections that are in nice agreement with the data. However, we stress the RGF is appropriate for the inclusive scattering where only the final lepton is detected, and thus can take into account also contributions that are not included in the experimental cross sections.

SUMMARY AND CONCLUSIONS

A deep understanding of the neutrino-nucleus cross sections is very important for the determination of neutrino oscillation parameters. Reliable theoretical models are required where all nuclear effects are well under control. Within the QE kinematics domain, the treatment of FSI is an essential ingredient for the comparison with data. In this contribution the RGF model for the inclusive QE electron and neutrino-nucleus scattering has been discussed. This model was originally developed for QE electron scattering, successfully tested in comparison with electron-scattering data, and then extended to neutrino-nucleus scattering. In the RGF model FSI are described in the inclusive scattering by the same complex optical potential as in the exclusive scattering, but the imaginary part is used in the two cases in a different way and in the inclusive process it is responsible for the redistribution of the flux in all the channels and the conservation of the flux. The RGF model gives results that are usually larger than results of other models based on the impulse approximation and that are in fair agreement with the CCQE MiniBooNE cross sections without the need to increase the standard value of the nucleon axial mass. However, the use of phenomenological optical potentials, does not allow us to disentangle the role of different reaction processes and explain in detail the

origin of the enhancement with respect of other models. The important role of contributions other than direct one-nucleon emission has been confirmed by different models; it has been observed that the neutrino-nucleus reaction at MiniBooNE can have significant contributions from effects beyond the IA in some kinematic regions where the experimental neutrino flux has significant strength. In Refs. [21, 35, 36, 37, 38, 39] the contribution of multinucleon excitations to CCQE scattering has been found sizable and able to bring the theory in agreement with the MiniBooNE cross sections without increasing the value of M_A . A critical review of nuclear effects in NCE and CCQE scattering is presented in [40]. Moreover, processes involving two-body currents, whose role is discussed in [41], should also be taken into account explicitly and consistently in a model to clarify the role of multinucleon emission. Fully relativistic microscopic calculations of two-particle-two-hole (2p-2h) contributions are extremely difficult and may be bound to model-dependent assumptions. The RGF results are also affected by uncertainties in the determination of the phenomenological optical potential. At present, lacking a phenomenological OP which exactly fulfills the dispersion relations in the whole energy region of interest, the RGF prediction is not univocally determined from the elastic phenomenology. A better determination of a phenomenological relativistic optical potential, which closely fulfills the dispersion relations, would be anyhow desirable and deserves further investigation.

REFERENCES

1. S. Boffi, C. Giusti, and F. D. Pacati, *Phys. Rept.* **226**, 1–101 (1993).
2. S. Boffi, C. Giusti, F. D. Pacati, and M. Radici, *Electromagnetic Response of Atomic Nuclei*, vol. 20 of *Oxford Studies in Nuclear Physics*, Clarendon Press, Oxford, 1996.
3. J. M. Udías, P. Sarriguren, E. Moya de Guerra, E. Garrido, and J. A. Caballero, *Phys. Rev. C* **48**, 2731–2739 (1993).
4. A. Meucci, C. Giusti, and F. D. Pacati, *Phys. Rev. C* **64**, 014604 (2001).
5. A. Meucci, C. Giusti, and F. D. Pacati, *Phys. Rev. C* **64**, 064615 (2001).
6. A. Meucci, *Phys. Rev. C* **65**, 044601 (2002).
7. M. Radici, A. Meucci, and W. H. Dickhoff, *Eur. Phys. J. A* **17**, 65–69 (2003).
8. C. Giusti, A. Meucci, F. D. Pacati, G. Co’, and V. De Donno, *Phys. Rev. C* **84**, 024615 (2011).
9. F. Capuzzi, C. Giusti, and F. D. Pacati, *Nucl. Phys. A* **524**, 681 – 705 (1991).
10. A. Meucci, F. Capuzzi, C. Giusti, and F. D. Pacati, *Phys. Rev. C* **67**, 054601 (2003).
11. A. Meucci, C. Giusti, and F. D. Pacati, *Nucl. Phys. A* **739**, 277–290 (2004).
12. F. Capuzzi, C. Giusti, F. D. Pacati, and D. N. Kadrev, *Ann. Phys. (N.Y.)* **317**, 492 – 529 (2005).
13. A. Meucci, C. Giusti, and F. D. Pacati, *Nucl. Phys. A* **756**, 359–381 (2005).
14. A. Meucci, C. Giusti, and F. D. Pacati, *Acta Phys. Polon. B* **37**, 2279–2286 (2006).
15. C. Giusti, A. Meucci, and F. D. Pacati, *Acta Phys. Polon. B* **40**, 2579–2584 (2009).
16. A. Meucci, J. A. Caballero, C. Giusti, F. D. Pacati, and J. M. Udías, *Phys. Rev. C* **80**, 024605 (2009).
17. A. Meucci, J. A. Caballero, C. Giusti, and J. M. Udías, *Phys. Rev. C* **83**, 064614 (2011).
18. A. Meucci, M. B. Barbaro, J. A. Caballero, C. Giusti, and J. M. Udías, *Phys. Rev. Lett.* **107**, 172501 (2011).
19. A. Meucci, and C. Giusti, *Phys. Rev. D* **85**, 093002 (2012).
20. A. A. Aguilar-Arevalo, et al., *Phys. Rev. D* **81**, 092005 (2010).
21. O. Benhar, P. Coletti, and D. Meloni, *Phys. Rev. Lett.* **105**, 132301 (2010).
22. A. V. Butkevich, *Phys. Rev. C* **82**, 055501 (2010).
23. C. Juszczak, J. T. Sobczyk, and J. Zmuda, *Phys. Rev. C* **82**, 045502 (2010).
24. J. A. Caballero, J. E. Amaro, M. B. Barbaro, T. W. Donnelly, C. Maieron, and J. M. Udías, *Phys. Rev. Lett.* **95**, 252502 (2005).
25. M. Anghinolfi, et al., *Nucl. Phys. A* **602**, 405 – 422 (1996).
26. D. B. Day, et al., *Phys. Rev. C* **48**, 1849–1863 (1993).
27. B. D. Serot, and J. D. Walecka, *Adv. Nucl. Phys.* **16**, 1–327 (1986).
28. E. D. Cooper, S. Hama, and B. C. Clark, *Phys. Rev. C* **80**, 034605 (2009).
29. A. A. Aguilar-Arevalo, et al. (2013), [arXiv:1301.7067](https://arxiv.org/abs/1301.7067).
30. A. A. Aguilar-Arevalo, et al., *Phys. Rev. D* **82**, 092005 (2010).
31. A. Meucci, C. Giusti, and F. D. Pacati, *Nucl. Phys. A* **744**, 307 – 322 (2004).
32. A. Meucci, C. Giusti, and F. D. Pacati, *Nucl. Phys. A* **773**, 250 – 262 (2006).
33. A. Meucci, C. Giusti, and F. D. Pacati, *Phys. Rev. C* **77**, 034606 (2008).
34. A. Meucci, C. Giusti, and F. D. Pacati, *Phys. Rev. D* **84**, 113003 (2011).
35. M. Martini, M. Ericson, G. Chanfray, and J. Marteau, *Phys. Rev. C* **81**, 045502 (2010).
36. M. Martini, M. Ericson, and G. Chanfray, *Phys. Rev. C* **84**, 055502 (2011).
37. J. Nieves, I. Ruiz Simo, and M. J. Vicente Vacas, *Phys. Rev. C* **83**, 045501 (2011).
38. J. Nieves, I. Ruiz Simo, and M. J. Vicente Vacas, *Phys. Lett. B* **707**, 72 – 75 (2012).
39. O. Lalakulich, K. Gallmeister, and U. Mosel, *Phys. Rev. C* **86**, 014614 (2012).
40. A. M. Ankowski, *Phys. Rev. C* **86**, 024616 (2012).
41. J. E. Amaro, M. B. Barbaro, J. A. Caballero, T. W. Donnelly, and J. M. Udías, *Phys. Rev. D* **84**, 033004 (2011).